AE International – Asia

Atmospheric Environment 38 (2004) 581–596

ATMOSPHERIC ENVIRONMENT

www.elsevier.com/locate/atmosenv

Analysis of tropospheric NO_x over Asia using the model of atmospheric transport and chemistry (MATCH-MPIC) and GOME-satellite observations

T. Kunhikrishnan[a,*], Mark G. Lawrence[a], Rolf von Kuhlmann[a], Andreas Richter[b], Annette Ladstätter-Weißenmayer[b], John P. Burrows[b]

[a] *Department of Atmospheric Chemistry, Max Planck Institute, Postfach 3060, D-55020 Mainz, Germany*
[b] *Institute of Environmental Physics and Remote Sensing, University of Bremen, Kufsteinerstr. 1, D-28359 Bremen, Germany*

Received 20 December 2002; received in revised form 11 September 2003; accepted 19 September 2003

Abstract

The distribution and budget of tropospheric NO_x over Asia, especially India, are examined using the global 3D chemistry–meteorology model MATCH-MPIC and GOME NO_2 columns. Enhanced abundances of NO_2 over China and northeast India are reproduced by the model, as are the pronounced maxima during biomass burning periods, though somewhat underestimated. The mean NO_2 column over India is also reproduced, though the model has trouble with the seasonal cycle for unknown reasons. Model sensitivity tests for the Indian region indicate that the scaled sensitivity to changes in the local NO_x source is 60–70% for lower tropospheric NO_x and is only 10–25% for tropospheric O_3, indicating that moderate reductions or increases in current NO_x emissions are not expected to lead to large changes in regional O_3 levels. In the upper troposphere, during winter nearly all of the NO_x comes from remote sources, while in summer deep convection causes the upper troposphere to become sensitive to local surface emissions ($\sim$40–50% scaled sensitivity) and lightning NO_x production ($\sim$10–20%). The regional lifetime of NO_x estimated for India, based on MATCH output is about 15–23 h, comparable to the lifetime of NO_x over China (14–21 h), while over Indonesia (23–43 h) and North Asia (21–47 h), it is longer and highly seasonal. Implications of these results are discussed.

Keywords: Nitrogen oxides; Asia; India; Lifetime; Regional emission strength; Satellite-model comparisons; Budget analysis

1. Introduction

The tropics play a key role in the chemistry of global troposphere. The region is photochemically active due to high levels of insolation and water vapor, and it dominates the oxidizing efficiency of the atmosphere with respect to many important gases such as CH_4. The tropics are also characterized by high and rapidly growing anthropogenic emissions of trace gases such as NO_x ($NO + NO_2$), SO_2 and hydrocarbons, especially from Asia.

This study focuses on NO_x over Asia, which includes India (5–35°N, 60–95°E) excluding the northern Himalayan region, a broad region of Indonesian Islands referred to here as Indonesia (10°S–20°N, 95–140°E), an extended Chinese region including Eastern Siberia called China (20–70°N, 95–150°E) and the northern-central part of Asia which includes mainly central Siberia and a part of former Russia, hereafter called North Asia (35–70°N, 60–95°E). (The schematic outline of the Asian domain chosen for this study is given below in Fig. 3.) NO_x influences the concentrations of greenhouse gases

*Corresponding author. Fax: +49-6131-305577.
E-mail address: kunhi@mpch-mainz.mpg.de (T. Kunhikrishnan).

1352-2310/$ - see front matter © 2003 Elsevier Ltd. All rights reserved.
doi:10.1016/j.atmosenv.2003.09.074

such as O_3, CH_4 and HFCs. Tropospheric NO_x catalyzes the production of O_3 and also stimulates production of OH radicals, which in turn initiate the breakdown of most key trace gases such as CH_4, CO, NMHCs and HFCs. NO_x has natural sources such as the production by lightning and microbiological processes in soils, as well as anthropogenic sources, especially fossil fuel combustion. The distributions and magnitudes of these sources are mostly poorly quantified.

Global total NO_x emissions are increasing, with the most rapid increase being in Asia. Kato and Akimoto (1992) reported that emissions from eastern Asia are increasing by about 4% per year. According to the study by Garg et al. (2001), NO_x emissions over the Indian region were 3.46 Tg (N)/yr in 1995, growing at an annual rate of 5.5%, with a substantial spatial heterogeneity. Similarly, Streets and Waldhoff (2000) compute that in the coming 25 years, industrial NO_x emissions from China are expected to double from 5 to 10.1 Tg(N)/yr. According to van Aardenne et al. (1999), in Asia, the emission of NO_x due to fossil fuel burning could increase even more rapidly, from about 6 Tg (N)/yr in 1990 to over 25 Tg (N/yr) in 2020, with China and India being the largest contributors. A recent study by Leue et al. (2001) has given a promising approach for the estimation of regional NO_x sources from satellite observations. They have estimated an annual NO_x source of 2.95, 2.70, 2.87 and 1.75 Tg for India, China, Indonesia and North Asia, respectively, and a global source of 43 ± 20 Tg (N)/yr for the period 1997. Wenig (2001) has reported an improved estimate of NO_x emissions from global ozone monitoring experiment (GOME) by applying a modified retrieval algorithm (personal communication, 2002), computing the mean NO_x emissions for the period 1996–2000 to be 1.87 Tg (India), 1.81 Tg (China), 2.59 Tg (Indonesia) and 3.82 Tg (North Asia). A significant amount of NO_x emissions from biomass burning over Asia has been reported in the recent years (Christopher et al., 1998; Ladstätter-Weißenmayer et al., 1999; Thompson et al., 2001). The increase in anthropogenic NO_x emissions and interannual variability of biomass burning will not only affect the urban air quality and the regional production of O_3 and OH but will also lead to increases in HNO_3 deposition in the Ocean basins, which may impact the biogeochemical cycling of nitrogen in marine and coastal ecosystems (Bey et al., 2001).

Our basic understanding of tropospheric NO_x over Asia is limited due to the lack of observations with sufficient spatial and temporal resolution. Moreover, especially in India, most of the present observations are available only in the major cities and will not be representative of the region as a whole. To supplement the missing information from in situ measurements, satellite observations and numerical models are needed to assess the chemical composition and key processes in the region.

The main objective of this study is to examine the characteristics of NO_x in the troposphere over Asia, especially over India, using output from the global model MATCH-MPIC along with satellite retrievals of the tropospheric NO_2 column from GOME. In the next section, the model and GOME retrieval technique are briefly described. Following that in Section 3, the model simulations are compared with GOME NO_2 observations. In Section 4, the model diagnostics of several key regional characteristics of tropospheric NO_x are considered; the mean tropospheric lifetime, the sensitivity of NO_x over India to emissions from the Indian region NO_x and from lightning and the impact of NO_x source perturbations on other trace gases such as O_3, HNO_3, PAN and OH over India. The uncertainties in computing the regional NO_x source strength based on satellite observations (Leue et al., 2001) are also discussed. The present study is the first examination of NO_x focusing on India and the surrounding region applying the combination of satellite tropospheric NO_2 column data together with global chemistry-transport model output.

2. Data source and methodology

2.1. Model description

MATCH-MPIC is the Max Planck Institute for Chemistry version of the Model for Atmospheric Chemistry and Transport-MATCH (Rasch et al., 1997). It is a global 3D offline model, which reads in gridded, time dependent values for the most basic meteorological parameters such as pressure, temperature and winds, and uses these to derive parameters like convective transport and cloud microphysics. The meteorology component simulates transport by advection, convection, dry turbulent mixing, cloud fraction, cloud water, and precipitation as well as the full tropospheric hydrological cycle. The input meteorological data used here is from the NCEP/NCAR reanalysis (Kalnay et al., 1996). The photochemistry component represents the major known sources, transformations and sinks of O_3 related gases including non-methane hydrocarbons. The oxides of nitrogen (NO and NO_2) are transported together, since the equilibrium processes determining their partitioning are much faster than the processes which affect the total NO_x concentration. Details of the meteorological and photochemical processes in MATCH-MPIC and their different versions are given by Lawrence et al. (1999) and von Kuhlmann et al. (2003a, b). The present study uses the model at a moderate horizontal resolution, T21 ($\sim 5.6^\circ$) with 28 vertical levels from the surface to 2.7 hPa in sigma coordinates. A 30-min model time step is used for this

study and the input meteorological data are interpolated to obtain the values for each time step.

The major NO_x sources in the atmosphere are fossil fuel combustion, biomass burning, lightning, and microbiological processes in the soil. Emission of NO_x is dominated by burning of fossil fuels including ship and aircraft emissions. There is a very large degree of uncertainty regarding the production by natural sources such as lightning (Lawrence et al., 1995; Price et al., 1997) and soils (Yienger and Levy, 1995). Biomass burning is also an important but uncertain source of NO_x (Galanter and Levy, 2000), which occurs primarily in the tropics.

The magnitudes of NO_x sources used in the MATCH-MPIC simulations are given in Table 1. The industrial source of NO_x used in MATCH-MPIC is based on the Emission Data base for Global Atmospheric Research-version 2.0 (EDGAR) $1^\circ \times 1^\circ$ emission inventories including ship NO_x emission based on Corbett et al. (1999). Biomass burning emissions are from Galanter and Levy (2000) and Andreae and Merlet (2001), and soil emissions are from Yienger and Levy (1995). The lightning NO_x source distribution is based on the parameterization of Price and Rind (1994), and aircraft emissions are from Baughcum et al. (1994). The average MATCH-MPIC NO_x source for India during 1997 is 1.72 Tg (N)/yr and has a maxima of 2.3 Tg (N)/yr during the month of April which is the dry summer period in India, in good agreement with the value of about 2 Tg (N)/yr mentioned in Section 1.

The loss processes of NO_x in MATCH include the reaction of NO_x with OH to form HNO_3 and the hydrolysis of N_2O_5 on aerosols and cloud droplets (following Dentener and Crutzen, 1993), as well as conversion to organic reservoir species. Physical loss of reactive nitrogen occurs by wet deposition (see Crutzen and Lawrence, 2000 for a description of the procedure) and by dry deposition (described in von Kuhlmann et al., 2003a).

The current version of the model has been extensively compared with observations of a number of species such as O_3, CO, non-methane hydrocarbons, nitrogen species and oxygenates (von Kuhlmann et al., 2003a, b). The model was found to reproduce most of the major observed features, such as seasonal cycles and vertical profiles in different parts of the world, land-sea gradients and the general abundance of many species. Some discrepancies, especially for oxygenated species, were also identified. The model has also been applied to examine the Asian region within Indian Ocean Experiment (INDOEX) and it has been shown that high tropospheric O_3 concentrations over the Arabian sea are reproduced by the model, which suggest substantial photochemical O_3 production in the outflow of Indian cities (Lal and Lawrence, 2001). MATCH-MPIC also reproduced the main spatial and temporal features of O_3 and CO distributions, especially the strong contrast between levels in the Arabian Sea and the south of ITCZ (Lawrence et al., 2003).

Table 1
Tropospheric sources of NO_x used in MATCH simulations and the estimated range as given by von Kuhlmann (2003a)

Source of NO_x	NO_x in Tg (N)/yr	Range in Tg (N)/yr
Industrial	24.1	16–30
Biomass burning	7.8	4–16
Soil	5.5	1.2–10
Lightning	2.8	2–16
Aircraft	0.45	0.5–0.6
Stratosphere	0.1	0.08–1
NH_3 oxidation	—	0.3–3
Oceans	—	<1

Total—40.75 Tg(N)/yr.

2.2. GOME

GOME is an instrument on board the ERS-2 satellite, which was launched by the European Space Agency in April 1995. ERS-2 is in a sun-synchronous orbit, approximately 800 km above Earth, crossing the equator at 10:30 local time in the descending (N–S) node. The GOME instrument observes the atmosphere in nadir view and global coverage is achieved in every 3 days after 43 orbits with a spatial resolution of 40 km latitude by 320 km longitude. The primary measurement quantity of GOME is the backscattered and reflected radiance in the wavelength region of 240–790 nm with a spectral resolution of 0.2–0.4 nm. From these measurements and the solar irradiance, which is measured once per day, trace gas total column amounts are retrieved utilizing the characteristic spectral absorption features. Although the main target species of GOME is ozone, other trace gases such as NO_2, BrO, HCHO or SO_2 can also be measured (Burrows et al., 1999; Burrows, 1999).

Detailed analysis of GOME NO_2 retrieval methods are given by Richter and Burrows (2000, 2002), Leue et al. (2001) and Martin et al. (2002). Briefly, column densities of NO_2 absorption are derived using the differential optical absorption spectroscopy (DOAS) technique. Separation of stratospheric and tropospheric contributions to the total NO_2 column is performed based on two basic assumptions, (i) the tropospheric column of NO_2 is negligible within the (oceanic) reference sector 180–170°W; (ii) NO_2 in the stratosphere is zonally symmetric. Therefore, the tropospheric column is obtained from the total column by subtracting the total column above the reference sector at the same latitude.

The vertical column density of the trace gas is obtained from the slant column density by computing a conversion factor called the air mass factor (AMF),

which varies with respect to solar zenith angle and the viewing geometry, the trace gas vertical profile as well as surface albedo and cloud cover. AMFs for the NO_2 column used for this study have been calculated with the radiative transfer model GOMETRAN (Rozanov et al., 1997) assuming clear sky conditions, a maritime aerosol layer, a surface albedo of 0.05 and a constant mixing ratio of NO_2 in the lower 1.5 km of the atmosphere (Richter and Burrows, 2002). One of the most important parameters for the calculation of the AMF is the cloud cover of the measurement pixel. The error in the calculation of AMF is estimated to be up to a factor of 2 for clear sky conditions with most NO_2 residing in the lower troposphere (surface—500 hPa, hereafter LT), where emissions are strongest, and will be more when clouds are present which hide the NO_2 below the cloud or when NO_2 is prevalent in the upper troposphere (500–150 hPa, hereafter UT). The data set used for this study considers only those pixels with a cloud cover below 0.1. From sensitivity studies and a validation with air-borne in situ measurements, the overall uncertainty in the tropospheric NO_2 column from GOME for a specific case is estimated to be up to 50% and is likely to be less in cloud-free conditions (Heland et al., 2002).

3. Seasonal NO_2 distributions over Asia from MATCH and GOME

Before comparing the MATCH-MPIC and GOME tropospheric NO_2 columns, we first verify the ability of the model to reproduce the GOME retrieval assumptions, and discuss the model output sampling issues for the polar orbiting satellite.

3.1. Model simulation of GOME retrieval assumptions

In this section we check whether the model computes the longitudinal homogeneity of the NO_2 column in the stratosphere, and we determine whether the tropospheric-NO_2 column over the reference sector 180–170°W is negligible. These are both explicit assumptions used to separate tropospheric and stratospheric NO_2 in the GOME retrieval. The range of mean monthly ratios of tropospheric to stratospheric NO_2 in the model simulation is very close to zero over the reference sector as expected. The model also simulates relatively low ratios over the Indian subcontinent (0.27–0.36), Indonesia (0.2–0.25) and China (0.3–0.5), which indicates one of the difficulties with tropospheric NO_2 retrievals, since the satellite has to look through a thick stratospheric column to see a much thinner tropospheric column. The assumption of zonal symmetry is generally valid in the model for the year 1997 for India, China, and Indonesia with an absolute mean deviation of 14%, 3.2% and 11.5%, respectively. However, there is a significant month-to-month variation, with a couple months of reaching as high as 30% regional absolute deviations. Thus applying the stratosphere-troposphere separation techniques to MATCH-MPIC should be rather accurate over longer periods, although a moderate uncertainty (20–30%) can be introduced into the results for individual months.

GOME samples the atmosphere at 10:30 local time. Since NO_2 has a regionally dependent diurnal cycle, we can expect that the ratio of NO_2 column at 10:30 versus the 24-h mean value varies with respect to space and time. We can examine the degree of this variation using MATCH. For instance, over India the ratio falls from $\sim$0.75 during winter to $\sim$0.58 during the summer monsoon (Fig. 1). Is this lower ratio due to the greater presence of clouds during summer monsoon? This would mean that the model clouds would have to be affecting NO_2 such that its value at 10:30 were suppressed compared to the diurnal cycle on a clear sky day. The main influence of clouds on the NO_2 column is by modifying the photolysis rates; clouds decrease the photolysis of NO_2 below, and thus increase its mixing ratio. To test this possibility, we performed a sensitivity run in which we neglected the effects of clouds in the photolysis rates computation (normally they are included on-line based on the technique of Landgraf and Crutzen, 1998). The 10:30/24-h ratios for this run are also plotted in Fig. 1 (dotted line). These are very close to the ratios (solid line) from the base run, with the exception of India and China during the summer monsoon (which is extremely cloudy), and Indonesia, which is very cloudy in summer as well as in winter. For India and China, the difference in the ratio in winter and summer is actually reduced by the cloud photolysis effects; thus it must be due to some other causes, such as differences in the length of day, or in the NO_x lifetime (discussed below). This sensitivity run also provides an indication of what would happen if we screened the model to only select cloud-free regions as is done with GOME data, since in the test run all regions are "cloud free" with respect to the photolysis rates. The difference in the ratio compared to base run (without the "effective cloud screening") is generally small over India, China and North Asia, suggesting that, unless the correlation between cloudiness and other effects (e.g., transport) on the diurnal cycle of NO_2 are large, a proper cloud screening will only yield a minor improvement. Over some regions (e.g., Indonesia), however the effect is larger, so that cloud screening might be worth testing in future studies.

3.2. Comparison of MATCH versus GOME NO_2 columns

The tropospheric NO_2 columns from GOME and MATCH-MPIC and the respective model NO_x

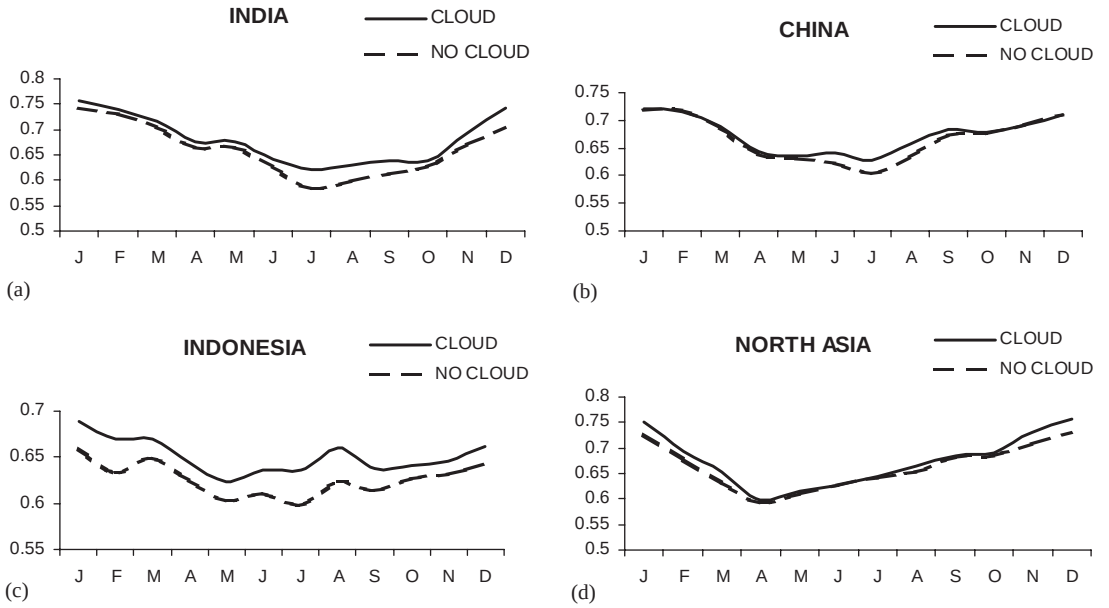

Fig. 1. Ratio of 10:30 local time to 24-h tropospheric NO_2 column (surface—150 hPa) from MATCH-MPIC for the base run and for a sensitivity run neglecting clouds in the photolysis rates computation for (a) India (5–35°N, 60–95°E), (b) China (20–70°N, 95–150°E), (c) Indonesia (10°S–20°N, 95–140°E), and (d) North Asia (35–70°N, 60–95°E).

emissions distribution for January and July 1997, for Asia, are given in Figs. 2 and 3. The model output and GOME observations show similar seasonal maxima with respect to different regions. The NO_x emissions from the source regions in Asia, mainly southeast China and northeast India are seen in Fig. 3 (note that surface emissions are greatest in April and least in October; not shown). We can also see notable emissions from north of Afghanistan including the Uzbekistan–Tajikistan and Kazakhstan area (~60–70°E, 35–45°N) during winter and summer over North Asia. Enhanced NO_2 abundances from GOME and MATCH during January and July are observed over China and north to northeast India. Over northern India, the simulated and observed NO_2 columns are greatest during January and less during the summer monsoon. The model underestimates the peak values over East Asia during January, but the East Asia peak during July is reproduced well. Even some smaller features are simulated well, such as the high values over Bangkok in January, and lower values in July.

Seasonal plots of the areal mean NO_2 column from the model and GOME for four subdomains of Asia are shown in Fig. 4. The mean modeled NO_2 as well as the maximum abundances for 1997–1998 (Table 2) is generally in agreement with the GOME NO_2 column in all the regions. The standard deviation is more than 50% of the magnitude of respective mass abundances from both GOME and MATCH. Over India, the month to month variations are not reproduced very well, while over the other regions the seasonal cycles and interannual variability are in much better agreement, although MATCH tends to underestimate the pronounced maxima during the biomass burning periods, especially over North Asia and China during the 1997–1998 El Nino. Part of the reason for the peak in January over North Asia is that the lifetime of NO_x is much longer in winter (see Fig. 7(c)). The figure also shows the relative enhancement of biomass burning over Indonesia during September 1997. As the Indonesia is considered as a broad region of all islands including maritime areas, the impact of biomass burning is reduced to less than one might expect if only land areas were considered. We have not been able to determine the reason for the discrepancies over the Indian region. The difference does not appear to be due to the effect of fractional land cover in the coastal grid cells on the NO_2 column. We have found, however, that the comparison is better over the central Indian region (Fig. 5), except far north over the Himalayas as shown in the grid-to-grid comparison in Fig. 6. Since the ratio of tropospheric to stratospheric NO_2 column is greatest over central India compared to the rest of India, it is possible that the retrieved tropospheric NO_2 column might be more accurate there. However, there are also several possible model errors (e.g., unaccounted chemical reactions, boundary layer mixing), which could be the cause, which can hopefully be determined in the future when more measurements are available for this region.

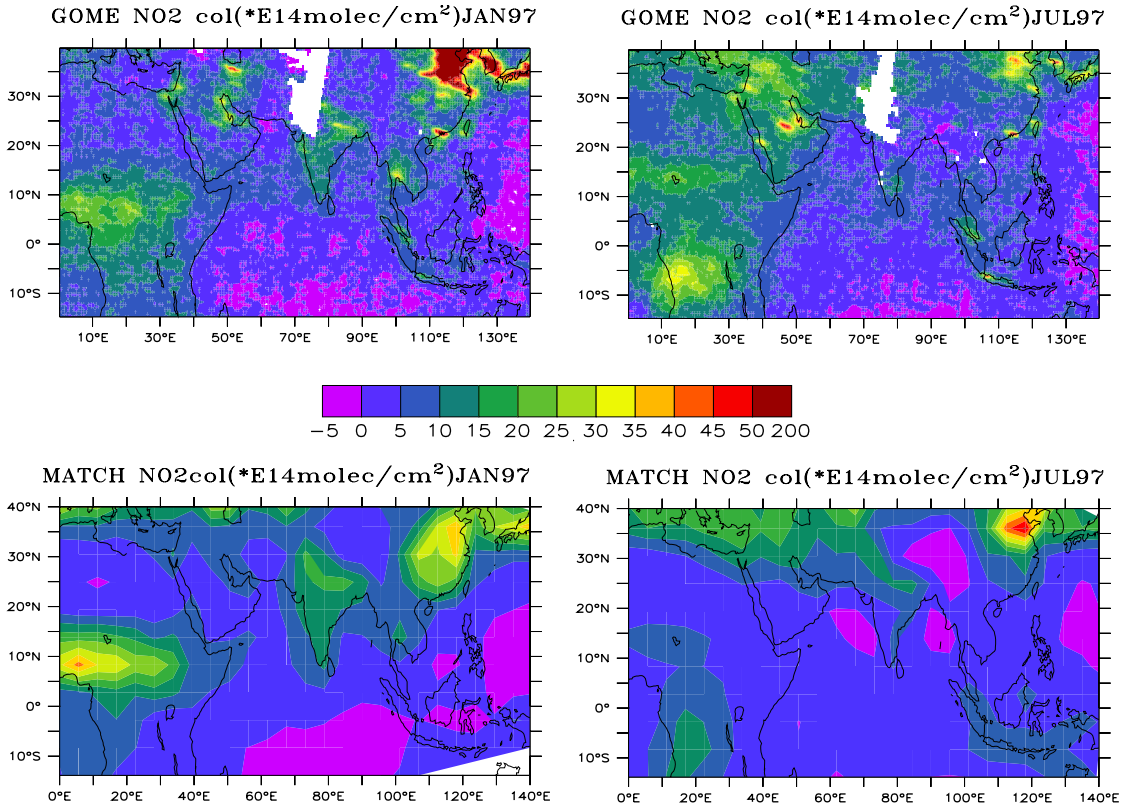

Fig. 2. NO_2 mass abundance from GOME and MATCH-MPIC for (a, b) January and (c, d) July 1997.

4. Model diagnostics of regional characteristics of tropospheric NO_x

In this section, we focus on the characteristics of regional NO_x chemistry over Asia such as the lifetime of NO_x, the sensitivity of tropospheric NO_x over India to local sources and lightning, and the impact of NO_x source perturbations on the abundances of different gases over India.

4.1. Lifetime of tropospheric NO_x over Asia

The lifetime of NO_x ($\tau(NO_x)$) plays an important role in tropospheric chemistry since it influences the amount of dispersion of NO_x to remote regions as well as the amount of O_3 which can be produced per emitted NO_x molecule. Knowledge of the NO_x lifetime is also necessary for the determination of the mean NO_x source strength from tropospheric NO_2 column measurements following Leue et al. (2001). The reaction of NO_x with OH to form HNO_3 is globally the most significant first order loss process (von Kuhlmann, 2003a), though other NO_x-removal reactions, especially conversion to N_2O_5 via $O_3 + NO_2 \rightarrow NO_3 + O_2$ and $NO_2 + NO_3 \rightarrow N_2O_5$ which then hydrolyzes to form HNO_3 (Dentener and Crutzen, 1993) can also contribute significantly, especially at night. Thus, the photochemical lifetime of NO_x depends strongly on the OH and O_3 concentrations. Furthermore, NO_x (as well as O_3 and OH) loss in the marine boundary layer (hereafter MBL) outflow region from India may be influenced by several poorly understood reaction mechanisms, especially those involving halogens (Dickerson et al., 1999; Andres Hernandez et al., 2001; Burkert et al., 2003). Similarly, complex reaction mechanisms involving aerosols in polluted populated regions may also contribute to NO_x loss. In this section, we use different approaches to estimate the $\tau(NO_x)$ over Asia, especially over India, based on MATCH-MPIC and GOME.

4.1.1. NO_x lifetime in the estimation of emissions from GOME data

The amount of a gas in steady state in a region is computed as the source to that region divided by the losses in or from the region. The sources can include direct emissions, chemical production, and transport into the region, while losses include chemical losses, deposition, and transport out of the region. If one

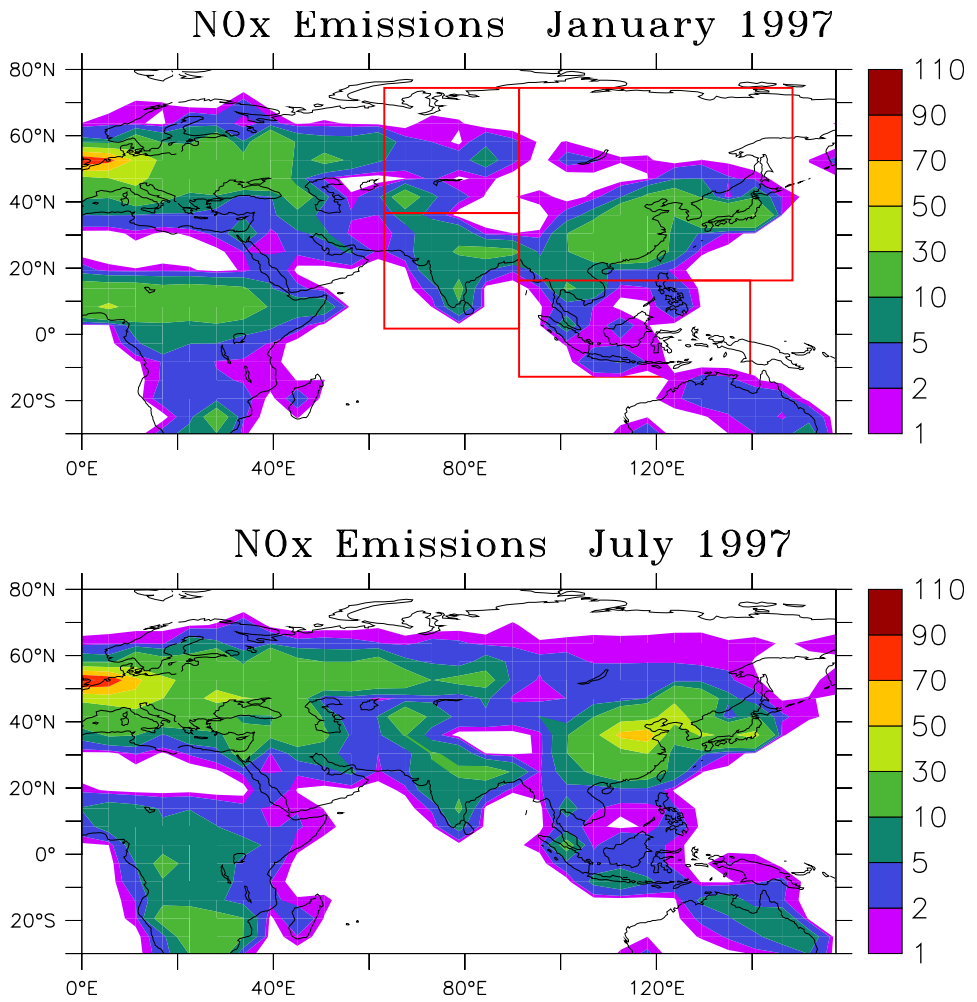

Fig. 3. Surface NO_x emission (10^{-12} kg/m^2/s) from MATCH-MPIC for January and July 1997. Schematic outline of Asian domains chosen for this study are clockwise from the bottom left: India, North Asia, China and Indonesia.

assumes that for a polluted region, the chemical production and transport sources are small relative to the emissions, and that the transport out of the region is small relative to the chemical and deposition losses, then it is possible to estimate the emissions of a gas as the ratio of its amount to its chemical lifetime, where the chemical lifetime is the inverse of the sum of the chemical and deposition losses. This approach (with these implicit assumptions) was used by Leue et al. (2001) to estimate regional NO_x emissions based on GOME data. They assumed $\tau(NO_x)$ of 27 h, estimated from the GOME data for the outflow of the eastern United States. Downwind of a source region, $\tau(NO_x)$ (due to chemical and deposition losses) can be estimated from the observed decay rate and the wind speed by making use of the fact that a gas in a Lagrangian parcel with no sources and a constant loss frequency L (NO_x), where $\tau(NO_x) = 1/L$ (NO_x), follows the equation

$$C = C_0 e^{-L(NO_x)t} = C_0 e^{-t/t(NO_x)},$$

where C_0 is the initial concentration and C is the concentration after a time t. Note that although NO_2 is observed by GOME, the decay will correspond approximately to $\tau(NO_x)$ due to fast recycling within the NO_x family. This assumes that any shift in the NO_2/NO_x ratio along the Lagrangian path is negligible. There are a number of other uncertainties in this approach. For instance, due to recycling of NO_x from HNO_3 and PAN, the lifetime estimate is an upper limit to the actual chemical lifetime. The presence of NO_2 in the free troposphere also causes the apparent decay rate in the MBL to be slower than it actually is. Furthermore, the lifetime in the outflow is not necessarily the same as the lifetime in the source region, and the implicit

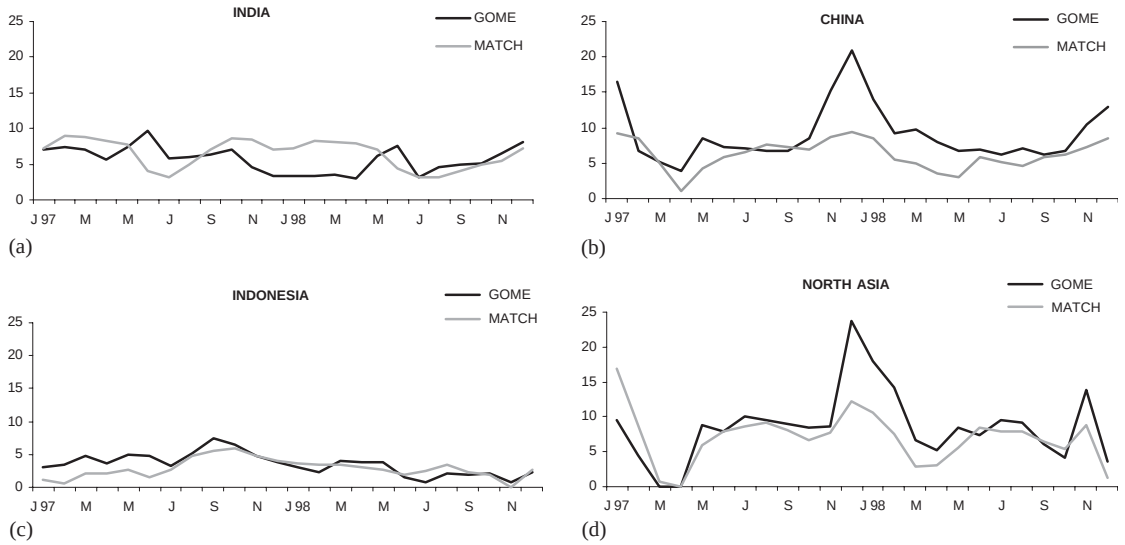

Fig. 4. Seasonal variation of areal mean of tropospheric NO_2 column (10^{14} molec/cm^2) over (a) India, (b) China, (c) Indonesia, and (d) North Asia from MATCH-MPIC and GOME.

Table 2
Mean tropospheric NO_2 column and their standard deviations for 1997–1998 computed from GOME and MATCH for Asia

Region	GOME abundance (10^{14} molecules/cm^2)			MATCH abundance (10^{14} molecules/cm^2)		
	Mean	Maximum	SD	Mean	Maximum	SD
India (5–35°N, 60–95°E)	5.68	9.6	2.0	6.48	12.6	1.82
China (20–70°N, 95–150°E)	9.05	20.8	4.05	6.21	12.8	2.09
Indonesia (10°S–20°N, 95–140°E)	3.49	7.4	1.65	2.84	8.7	1.33
North Asia (35–70°N, 60–95°E)	8.61	23.7	5.17	7.05	23.1	3.72

assumption that export losses are small compared to chemical losses and is not valid for all regions. Finally, the lifetime varies from region to region, depending on chemical activity.

To examine regional variations, we have computed the lifetime in the outflow from India in a similar manner to Leue et al. (2001) with the exception that we have taken in to account the varying offshore wind speed at 850 hPa from NCEP monthly mean data, whereas Leue et al. (2001) assumed a constant wind speed of 6 m/s. The only appropriate period for such a computation for Indian region is the NE monsoon (January) when the winds are steadily offshore (Fig. 7). The method is employed for January 1997 over the Arabian Sea along different inclinations (31°, 45° and 49°) from a source location (72.75°E, 19.25°N) near Mumbai (west coast of India) with an initial NO_2 column of 2.2×10^{15} molecules/cm^2. The analysis of decay over the region is limited to about 400–700 km for a single direction, because the air eventually encounters the African and Arabian outflow seen in the GOME observations. Fig. 8(a) shows the decay as a function of time for the three trajectory angles. The mean lifetime of NO_x from GOME computed in this way is equal to 18.2 h, in good agreement for all three trajectories. This lifetime is considerably lower than the value of 27 h computed by Leue et al. (2001) for the US East coast. The difference is likely due to greater chemical activity in the tropics, due to high levels of solar insolation, temperature and OH concentrations. One implication of this is that the NO_x in the US outflow has a longer time over which ozone production and long-range transport can occur. This large regional difference in $\tau(NO_x)$ based on the GOME data indicates the importance of using regionally appropriate lifetimes to estimate emissions. Unfortunately, these are not known well. The GOME decay curve method can only be applied to a few outflow regions worldwide, and cannot be applied to the source regions themselves. For this, we must currently rely on model analyses, as discussed in the following section.

4.1.2. *Lifetime of tropospheric NO_x over India and the Arabian Sea from MATCH-MPIC*

First, we have investigated whether MATCH computes a similar lifetime in the Indian outflow to that

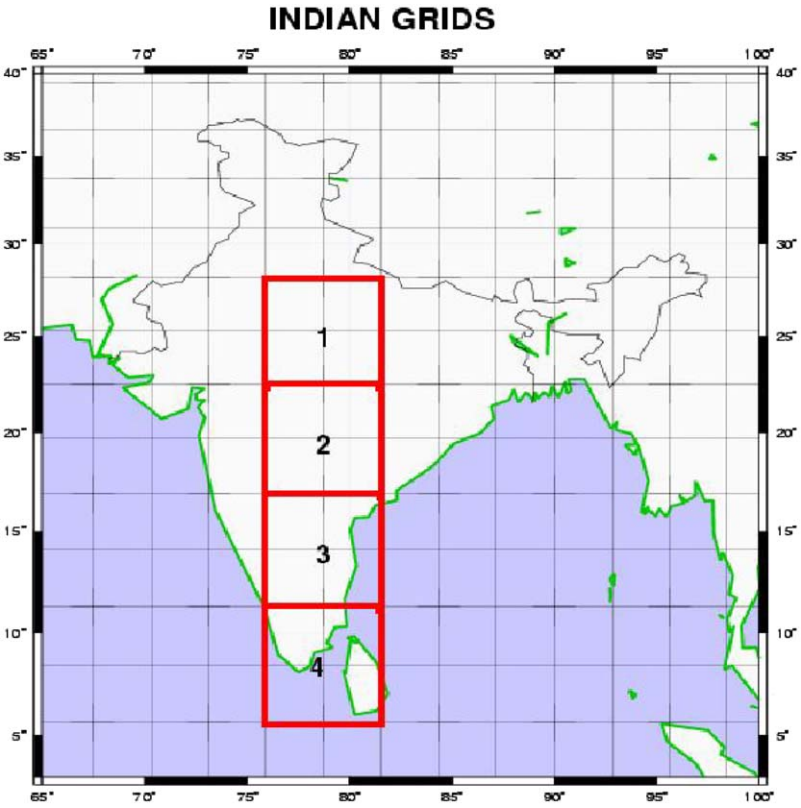

Fig. 5. Indian region for grid-to-grid comparison along 78.8°E of GOME and MATCH-MPIC.

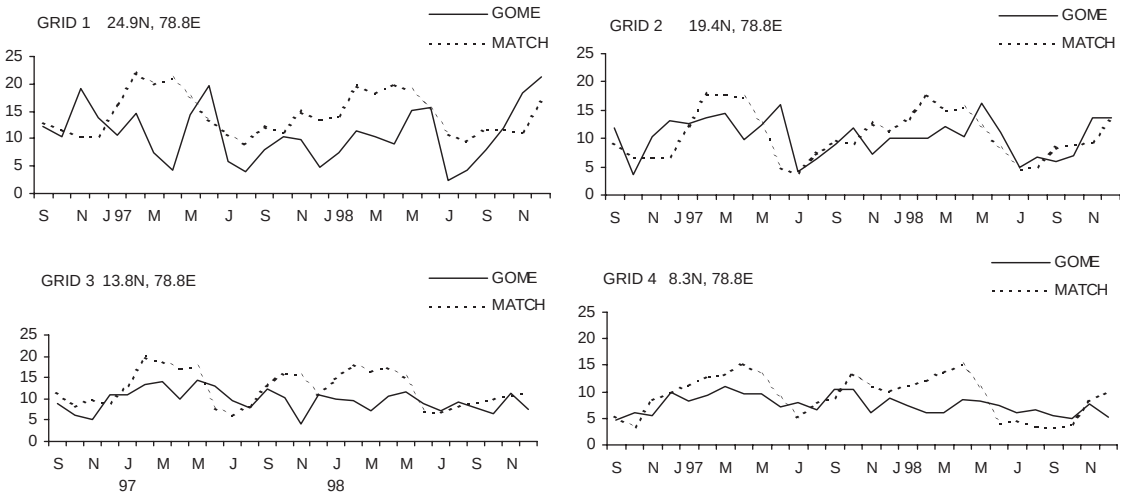

Fig. 6. Grid-to-grid comparison of GOME and MATCH-MPIC; all GOME pixels falling within each model grid (depicted in Fig. 5) are averaged for the comparison.

estimated from the tropospheric NO_2 observed by GOME. Unfortunately, this cannot be done with the same decay curve method, since even at our highest resolution (T63, i.e., $1.9^\circ \times 1.9^\circ$); the model output is still too noisy to determine a clear exponential decay rate. Instead, we determine the lifetime based on the primary chemical loss process, reaction of NO_2 with OH to form HNO_3. The reaction rate coefficient 'k' for

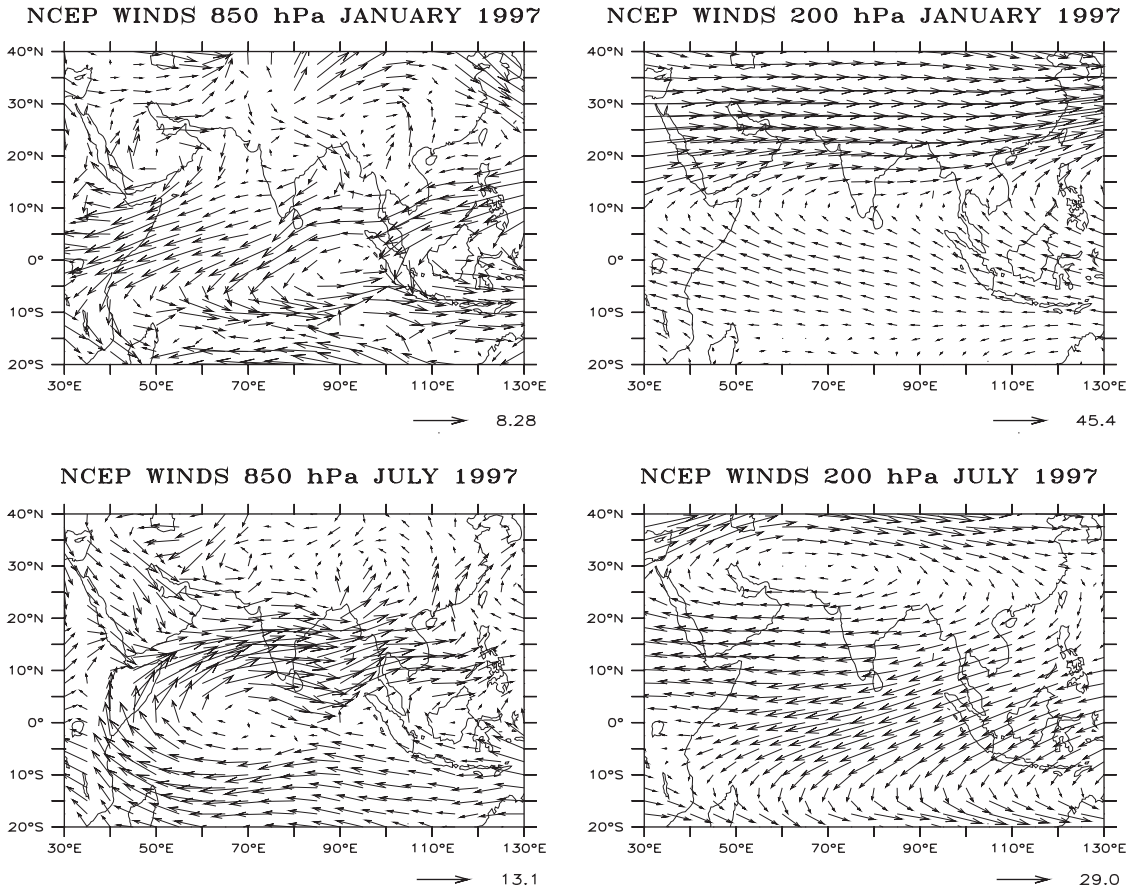

Fig. 7. Mean wind fields during the winter monsoon (January) and the summer monsoon (July) over the Indian region for 850 and 200 hPa for 1997.

$OH + NO_2 \rightarrow HNO_3$ is computed using the function given by Brown et al. (1999). In the MBL over the Arabian Sea, in the 6 grid cells in the examined outflow region, the lifetime in MATCH for NO_2 loss to HNO_3 is 16.1 h. This is consistent with the GOME data, given the uncertainties discussed above, particularly considering that both are upper limits (for the MATCH estimates this is because other losses, such as N_2O_5 on aerosols, also contribute).

Second, we consider $\tau(NO_x)$ computed by MATCH for India. $\tau(NO_x)$ is computed as the ratio of total NO_x mass abundance over the continental Indian region to the integrated loss rate for the region, based on output from the model budget routines for loss processes of NO_x due to the photochemistry and dry deposition, which are archived for India. It is found that the mean $\tau(NO_x)$ over India is in the range of 16.0–23.1 h with a mean value of 18.3 h (Fig. 8(b)), which interestingly, is close to $\tau(NO_x)$ computed above for the outflow. The minimum values are during February–April, when the sunshine is maximum over India and the highest values are during October–November.

Finally, we consider the lifetime of NO_x over other Asian regions. We did not have model budget output for these regions, but can use another approximation. In steady state in a closed region the integrated loss rate is equal to the total emission rate over the region. Therefore in regions where detailed model budget output is not available, an estimate of the average lifetime of NO_x can be made from the ratio of mass abundance to the total emission from the region provided the net transport of NO_x into the region is small. This technique works fairly well for India, as can be seen in Fig. 8(b) by the agreement with the lifetime (for the same region) computed using the model output. The mean lifetimes of NO_x over India, China, Indonesia, and north Asia computed by the same method are shown in the Fig. 8(c). The lifetime of NO_x over China (17.3 [14–21] hours) is comparable to India with little seasonal variability. In contrast, the lifetimes of NO_x over Indonesia (31.4 [23–43] hours) and North Asia (29.5 [21–47] hours) are nearly a factor of two longer and highly seasonal, emphasizing the regional variability of $\tau(NO_x)$. The longer lifetime over Indonesia is mainly

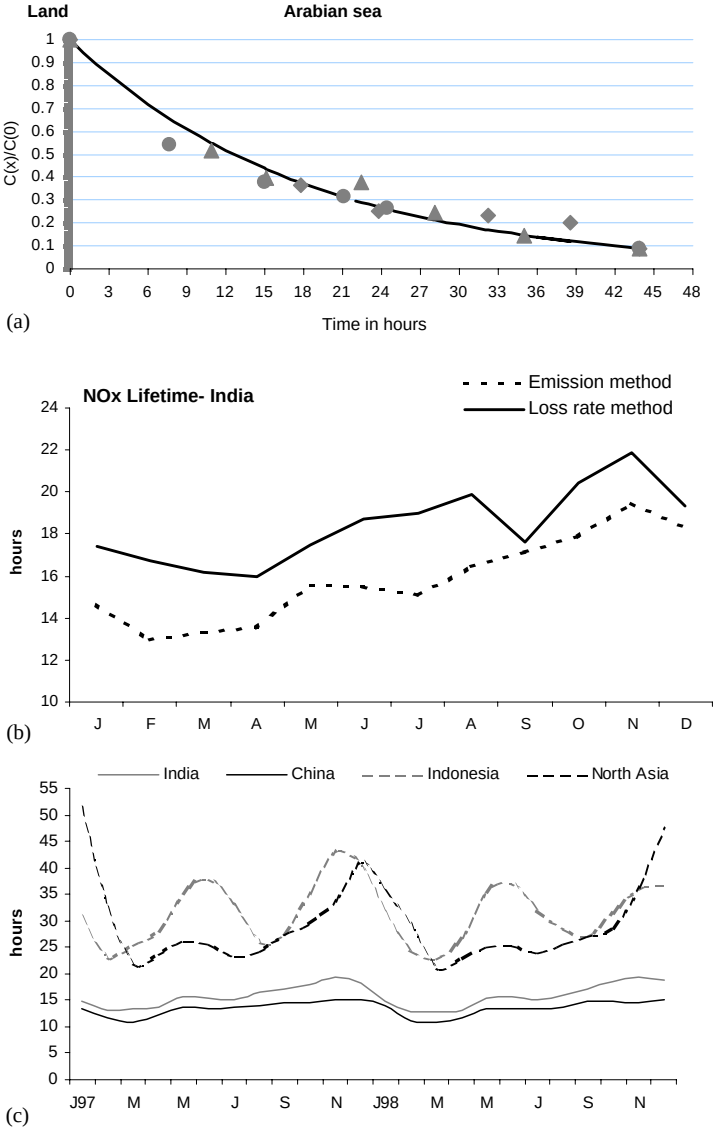

Fig. 8. Tropospheric lifetime of NO_x. (a) Over Arabian Sea outflow region from decay curve method—ratio of NO_2 concentration to the initial one (from GOME) with respect to time from the source location (72.75°E, 19.25°N) over the west coast of India through Arabian Sea during January 1997. (b) Over India by using the loss-rate method (solid line) based on model budget analysis and emission (dotted line) from India. (c) Over India, China, North Asia and Indonesia by using emission method from MATCH.

due to lower O_3, OH, and aerosol levels as compared to China and India, which makes the loss less efficient over Indonesia, which in turn is partly due to the region including both land and ocean areas.

4.2. Sensitivity of NO_x over India to local emissions

In this section we examine the extent to which the Indian NO_x is sensitive to local Indian emissions. We have not determined the individual source attributions, which require tagged NO_y tracers (which MATCH-MPIC is not currently set up to do). Instead we determine the "scaled sensitivity" to local emissions (i.e., the extrapolation of the first derivative of changes in the emissions) which provides information that is relevant for pollution mitigation efforts as well as for top-down approaches to quantify the local NO_x sources over the region, by using GOME data as introduced in Leue et al (2001). For this we have performed two test runs.

(i) NO_x emissions from the Indian region (all sources) set to 90% of its base source (i.e., 10% reduction in

the source strength) and unchanged for the rest of the world.

(ii) As (i) except including normal lightning NO_x emission from the Indian region.

The output is compared with the standard model run (base run) to examine the contribution of Indian region emissions; the results from (ii) can be compared with (i) to indicate specifically the role of lightning NO_x over Indian region. In both cases, the change in NO_x is multiplied by 10 to determine the scaled sensitivity (%) to changes in local NO_x emissions.

We find (Fig. 9(a)) that the scaled sensitivity of the LT NO_x over India to local emissions is 60–70%. If NO_x were a linear tracer with only local sources, the scaled sensitivity would be 100%. The reduced sensitivity is caused in part by remote sources, and in part by the feedback with OH. This feedback is generally negative: reduced NO_x levels lead to reduced OH concentrations (except in regions with very high NO_x levels and/or high NO_x to hydrocarbon ratios, which is not expected to apply to India), which in turn increases the NO_x lifetime, so that the actual reduction in NO_x is not as large as without the feedback. Other chemical feedbacks, such as via O_3 and N_2O_5 hydrolysis, can have similar effects. The largest sensitivity to NO_x from India is during winter months due to the lowest OH levels and strong boundary layer inversion with little mixing and subsidence, whereas in summer OH levels are higher and more NO_x is transported away by strong boundary layer mixing and convection, and the air is replaced by the strong LT inflow from the west/southwest (Fig. 7). Since these runs give the upper bound to remote sources (due to the OH-lifetime feedback), this suggests that the contribution from remote sources to the LT (<30–40%) is not likely to introduce a large error into the determination of regional NO_x emission strength from satellite data as applied by Leue et al.(2001).

In the UT, on the other hand, the scaled sensitivity to local NO_x sources is highly seasonal with a minimum of about 5% during winter months, when little NO_x is transported vertically into the UT, and when strong westerlies prevail, which should carry considerable NO_x emissions as PAN or HNO_3 that have reached the UT by warm conveyor belts (as shown in Stohl, 2001). This will introduce an uncertainty into the regional emissions determination following Leue et al. (2001). In contrast, during summer, horizontal transport of NO_x from remote sources is weaker, and the scaled sensitivity to local emission is 60–70% in the UT. This is partly due to the strong summer monsoon convection carrying surface emissions directly to the UT. Lightning also contributes to the NO_x column during the summer monsoon, as discussed in the next section. Much of the remote source

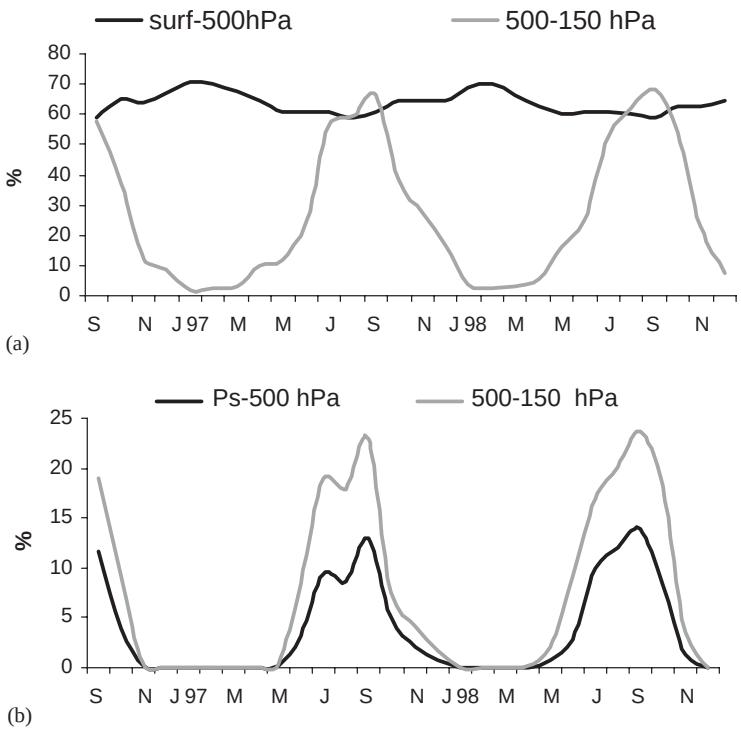

Fig. 9. Scaled sensitivity of NO_x from (a) local source and (b) lightning NO_x for surface—500 hPa (dark line), and for 500–150 hPa (grey line).

during summer is expected to be due to convection lifting pollutants from South East Asia, which are then transported over India by the tropical easterly jet (Fig. 7).

4.3. NO_x emission from lightning

Lightning associated with thunderstorms occurs in different parts of India during summer, mainly in March–May, and in the monsoon period June–September. Similarly, during the post-monsoon season (October and November) in association with cyclonic storms and depressions thunderstorms occur, mostly over peninsular India. Except over northwest India, in association with western disturbances, thunderstorms are rare in winter (December–February). Here we examine the model-computed NO_x from lightning discharges over India. The sensitivity run shows that lightning NO_x production (Fig. 9(b)) over the Indian region contributes significantly during the summer period (negligible during the winter). During the September–October, lightning is responsible for an increase of up to 12% of NO_x amounts in the LT and about 20% in the UT (500–150 hPa). It is noted however that the model does not simulate the anticipated increase of NO_x emission during the March–April period, when large-scale thunderstorm activities are common over India (FMU report, India Meteorological Department, 1973).

4.4. Impact of NO_x source perturbations on the abundances of O_3, HNO_3, OH and PAN over the Indian region

The impact of a NO_x source perturbation in a sensitivity run with a 10% increase in Indian NO_x emissions on the abundance of other key gases is examined to understand the role of local NO_x emissions on the chemical composition of the LT and UT (Fig. 10) of the Indian region (note that the results are nearly identical in reverse for the 10% decrease run). The scaled sensitivity of NO_x as noted in Section 4.2 is about 60–70% in the LT (all year) and in the UT in summer. Most gases respond to the change in NO_x in the LT with a smaller change, i.e., the scaled sensitivity of O_3, OH and PAN are 10–30%, 30–50% and 50–60%, respectively. HNO_3 is an interesting exception, with a scaled sensitivity (50–100%) sometimes exceeding that of NO_x, and with a strong seasonal variation due to its high solubility. The strong enhancement of HNO_3 against an increase in NO_x is mainly due to the increase in the formation of HNO_3 by the reaction of NO_2 with OH (since OH also increases). The variations of all the gases over the UT are highly seasonal, corresponding to the

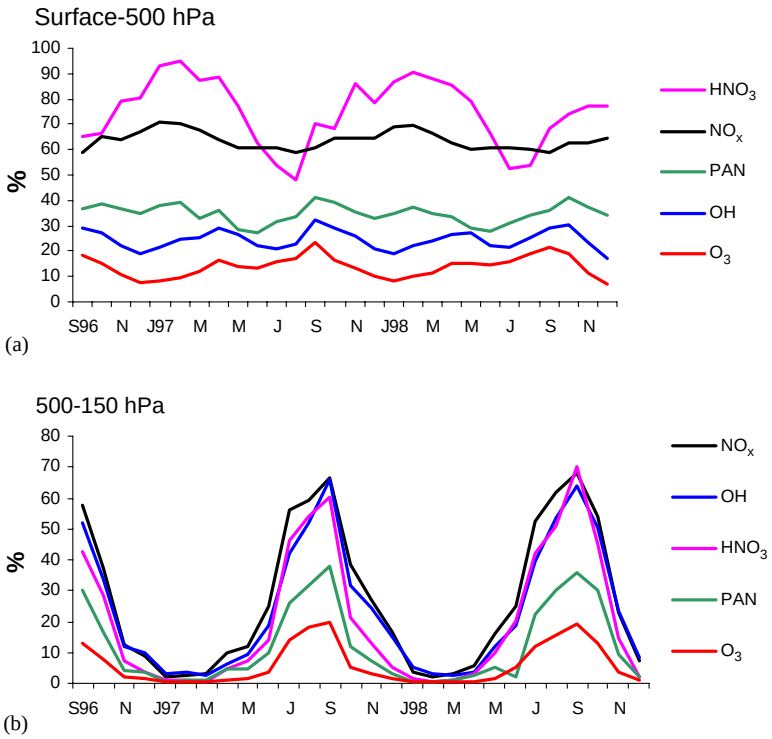

Fig. 10. Scaled sensitivity (%) of NO_x, HNO_3, PAN, OH and O_3 with respect to changes in the NO_x source strength over India for (a) lower troposphere (surface—500 hPa), (b) upper troposphere (500–150 hPa).

seasonal variation of NO_x. The rather low scaled sensitivity of O_3 indicates that it is not strongly controlled by changes in NO_x. We also similarly checked the scaled sensitivity to increases in non-methane hydrocarbon (NMHC) sources over India, and found it to be $\leqslant 15\%$ (not shown). Thus while O_3 over India is more sensitive to changes in NO_x than in hydrocarbons, it is not very sensitive to either.

5. Concluding remarks

In this study we have examined the characteristics of tropospheric NO_x over Asia, with a focus on India, using the 3D global transport model MATCH-MPIC together with the NO_2 column derived from GOME satellite data. The model is able to simulate the GOME-NO_2 retrieval assumptions such as the longitudinal homogeneity of the NO_2 column in the stratosphere, and a negligible amount of tropospheric NO_2 in the Pacific oceanic reference sector. The sampling time correction factor between modeled 24-h mean NO_2 column and 10:30 local time is highly variable with respect to time and space. This implies that it is difficult to extrapolate from the GOME NO_2 measurements to 24 h or monthly mean values without the aid of information on diurnal cycles from a global model. In general, the seasonal average NO_2 column from MATCH and GOME are comparable in magnitude, although the model shows some significant discrepancies in the month to month variations over India, which we cannot explain yet; over the other Asian regions the seasonal cycles and interannual variability are in much better agreement; in particular MATCH reproduces the pronounced maxima during the biomass burning periods, especially over North Asia and China, but tends to underestimate their magnitudes.

According to the model simulations, the scaled sensitivity of LT NO_x over India to changes in local NO_x emissions is 60–70%, indicating that regional NO_x is mainly sensitive to local emissions, but that a given relative change in these emissions leads to a 30–40% smaller relative change in NO_x levels due to import from remote sources and to chemical feedback effects. The scaled sensitivity for NO_x in the summertime UT is similar, due to convective lifting of pollutants, while the wintertime UT is almost completely insensitive to local sources. We found that UT-NO_x is less than 10% to 20% of the total tropospheric column during winter; however, it was 30%–40% during summer. The study indicates that a non-negligible contribution of NO_x is from remote sources to the tropospheric column (surface—150 hPa), and introduces an uncertainty into the determination of the regional NO_x source strength using GOME data following the technique of Leue et al. (2001). Sensitivity studies show that lightning NO_x production over India has a strong seasonality and increases NO_x by 10–20% during the summer. The test runs also showed that O_3, OH and PAN over the Indian region have smaller scaled sensitivities (10–25%, 30–50% and 50–60%, respectively) than NO_x, while the scaled sensitivity of HNO_3 exceeded that of NO_x (up to a 100%), due to nonlinearities in the chemical system. The relative insensitivity computed for O_3 in the LT over the Indian continent with respect to changes in the emissions of NO_x ($<25\%$ scaled sensitivity) and NMHCs ($<15\%$ scaled sensitivity) indicates that it may be difficult to reduce regional O_3 levels to considerably below present levels without extreme emissions reductions, while on the other hand moderate increases in NO_x and hydrocarbon emissions would not be expected to lead to large increases in regional O_3. This does not apply, however, to large increases, such as a doubling of NO_x emissions, which might result in a change in the chemical regime and potentially much larger O_3 increases.

The regional lifetime of NO_x estimated for the Indian subcontinent, based on MATCH, is about 15–23 h. The estimated lifetime over the Arabian Sea outflow from GOME is 18.2 h and is consistent with the value (16.1 h) computed for the 6 grids of MATCH over the outflow region in the MBL from Mumbai. This value is shorter than the 27 h computed in Leue et al. (2001) for the US east coast (using the same technique with GOME data). Over other Asian areas, we compute mean lifetimes of 17.4 h for China, 31.4 h for Indonesia and 29.5 h for North Asia. This large regional difference in the NO_x lifetime based on the GOME and MATCH data indicates the importance of using regionally appropriate lifetimes for NO_x to estimate emissions and also emphasizes that the degree of outflow of pollutants depends not only on the magnitudes of local emissions, but also on the local chemistry and meteorology which determine pollutant lifetimes.

Acknowledgements

The first author is grateful to India Meteorological Department, M/o. Science and Technology, Government of India for granting leave for doing his studies at MPIC, Mainz. The first author is also grateful to Prof. P.J. Crutzen and Prof. Jos Lelieveld for their encouragement. We are thankful to Phil Rasch, NCAR, Boulder, USA, for providing and supporting MATCH. Thanks are due to Patrick Jöckel, Marc Salzmann, Lorenzo Labrador and Mark Weber for useful discussions. The technical assistance provided by Jörg Steinkamp is appreciated. We acknowledge funding for the work at the MPI from the German Ministry of Education and Research (BMBF), project 07-ATC-02 and for the University of Bremen from the state of

Bremen, the European Union, the BMBF and the German Space Agency (DLR).

References

Andreae, M.O., Merlet, P., 2001. Emission of trace gases and aerosols from biomass burning. Global Biogeochemical Cycles 15, 955–966.

Andres Hernandez, M.D., Burkert, J., Reichert, L., Stöbener, D., Meyer-Arnek, J., Burrows, J.P., Dickerson, R.R., Doddridge, B.G., 2001. Marine boundary layer peroxy radical chemistry during the AEROSOL 99 campaign: measurments and analysis. Journal of Geophysical Research 106, 20833–20846.

Baughcum, S.L., Henderson, S.C., Hertel, P.S., Maggiora, D.R., Oncina, C.A., 1994. Stratospheric emissions effects database development. Contr. rep. cr-4592, NASA.

Bey, I., Jacob, D.J., Yantosca, R.M., Logan, J.A., Yantosca, R.M., 2001. Asian chemical outflow to the Pacific in spring: origions, pathways, and budgets. Journal of Geophysical Research 106, 23097–23114.

Brown, S., Talukdar, R., Ravishankara, A., 1999. Rate constants for the reaction $OH + NO_2 + M \rightarrow HNO_3 + M$ under atmospheric conditions. Chemical Physics Letters 299, 277–284.

Burkert, J., Andreas-Hernandez, M., Reichert, L., Meyer-Arnek, J., Doddridge, B., Dickerson, R.R., Mühle, J., Zahn, A., Carsey, T., Burrows, J.P., 2003. Trace gas and radical diurnal behaviour in the marine boundary layer during INDOEX 1999. Journal of Geophysical Research 108 (D8), doi:10.1029/2002JD002790.

Burrows, J.P., 1999. Current and future passive remote sensing techniques used to determine atmospheric constituents. In: Bouwman, A.F. (Ed.), Approaches to Scaling Trace Gas Fluxes in Ecosystems, Developments in Atmospheric Sciences 24. Elsevier, Amsterdam, pp. 315–347 (ISBN 0-444-82934-2.).

Burrows, J.P., Weber, M., Buchwitz, M., Rozanov, V.V., Ladstätter-Weißenmayer, A., Richter, A., DeBeek, R., Hoogen, R., Brmstedt, K., Eichmann, K.U., 1999. The global ozone monitoring experiment (GOME): mission concept and first scientific results. Journal of Atmospheric Science 56, 151–175.

Christopher, S.A., Chou, J., Welch, R.M., Kliche, D.V., Connors, V.S., 1998. Satellite investigations of fire, smoke, and carbon monoxide during April 1994 MAPS mission: case studies over tropical Asia. Journal of Geophysical Research 103, 19327–19336.

Corbett, J.J., Fischbeck, P.S., Pandis, S.N., 1999. Global nitrogen and sulfur inventories for oceangoing ships. Journal of Geophysical Research 104, 3457–3470.

Crutzen, P.J., Lawrence, M.G., 2000. The impact of precipitation scavenging on the transport of trace gases: a 3-dimensional model sensitivity study. Journal of Atmospheric Chemistry 37, 81–112.

Dentener, F.J., Crutzen, P.J., 1993. Reaction of N_2O_5 on tropospheric aerosols: impact on the global distributions of NO_x, O_3, and OH. Journal of Geophysical Research 98, 7149–7163.

Dickerson, R.R., Rhoads, K.P., Carsey, T.P., Oltmans, S.J., Burrows, J.P., Crutzen, P.J., 1999. Ozone in the remote marine boundary layer: a possible role for halogens. Journal of Geophysical Research 104, 21385–21395.

Galanter, M., Levy, H., Carmichael, G.R., 2000. Impacts of biomass burning on tropospheric CO NO_x and O_3. Journal of Geophysical Research 105, 6633–6653.

Garg, A., Shukla, P.R., Bhattacharya, S., Dadhwal, V.K., 2001. Sub-region (district) and sector level SO_2 and NO_x emissions for India—assessment of inventories and mitigation flexibility. Atmospheric Environment 35, 703–713.

Heland, J., Schlager, H., Richter, A., Burrows, J.P., 2002. First comparison of tropospheric NO_2 column densities retrieved from GOME measurements and in situ aircraft profile measurements. Geophysical Research Letters 29(20), 1983 (doi:10.1029/2002GL015528).

Kalnay, E., Kanamitsu, M., Kirstler, R., Collins, W., Deaven, D., Gandin, L., Iredell, M., Saha, S., White, G., Woollen, J., Zhu, Y., Chelliah, M., Ebisuzaki, W., Higgins, W., Janowiak, J., Mo, K., Ropelewski, C.J.W., Leetmaa, A., Reynolds, R., Jenne, R., Joseph, D., 1996. The NCEP/NCAR 40-year reanalysis project. Bulletin of the American Meteorological Society 77, 437–471.

Kato, N., Akimoto, H., 1992. Anthropogenic emissions of SO_2 and NO_x in Asia: emissions inventories (plus errata). Atmospheric Environment 26A, 2997–3017.

Ladstätter-Weißenmayer, A., Burrows, J.P., Crutzen, P.J., Richter, A., 1999. Biomass burning and its influence on the troposphere: atmospheric measurements from space. ESA WPP 161, 1369–1374.

Lal, S., Lawrence, M.G., 2001. Elevated mixing ratios of surface ozone over the Arabian Sea. Geophysical Research Letters 28, 1487–1490.

Landgraf, J., Crutzen, P.J., 1998. An efficient method for online calculations of photolysis and heating rates. Journal of Atmospheric Science 55, 863–878.

Lawrence, M.G., Chameides, W.L., Kasibhatla, P.S., Levy II, H., Moxim.M., 1995. Lightning and Atmospheric Chemistry: The Rate of Atmospheric NO Production, Vol. I. CRC Press, Boca Raton, FL, pp. 189–202.

Lawrence, M.G., Crutzen, P.J., Rasch, P.J., Eaton, B.E., Mahowald, N.M., 1999. A model for studies of tropospheric photochemistry: description, global distributions, evaluation. Journal of Geophysical Research 104, 26245–26277.

Lawrence, M.G., Rasch, P.J., von Kuhlmann, R., Williams, J., Fischer, J., Reus M, de., Lelieveld, J., Schultz, M., Stier, P., Huntrieser, H., Heland, J., Stohl, A., Forster, C., Elbern, H., Jakobs, H., Dickerson, R., 2003. Global chemical weather forecasts for field campaign planning: predictions and observations of large-scale features during INDOEX, MINOS, and CONTRACE. Atmospheric Chemistry and Physics 3, 267–289.

Leue, C., Wenig, M., Wagner, T., Klimm, O., Platt, U., Jähne, B., 2001. Quantitative analysis of NO_x emission from global ozone monitoring experiment satellite image sequences. Journal of Geophysical Research 106 (D6), 5493.

Martin, R.V., Chance, K., Jacob, D.J., Kurosu, T.P., Spurr, R.J.D., Bucsela, E., Gleason, J.F., Palmer, P.I., Bey, I., Fiore, A.M., Li, Q., Yantosca, R.M., Koelemeijer, R.B.A., 2002. An improved retrieval of tropospheric nitrogen

dioxide from GOME. Journal of Geophysical Research 107 (D20), 4437 (doi:10.1029JD001027).

Price, C., Rind, D., 1994. Modeling global lightning distribution in a general circulation model. Monthly Weather Review 122, 1930–1939.

Price, C., Penner, J., Prather, M., 1997. NO_x from lightning, Part I and II: global distribution based on lightning physics. Journal of Geophysical Research 102, 5929–5951.

Rasch, P.J., Mahowald, N.M., Eaton, B.E., 1997. Representations of transport, convection and the hydrologic cycle in chemical transport models: implications for the modeling of short lived and soluble species. Journal of Geophysical Research 102(28), 127–128, 138.

Richter, A., Burrows, J.P., 2000. A multi wavelength approach for the retrieval of tropospheric NO_2 from GOME measurements. ERS-Envisat Symposium "Looking down to earth in the new Millennium", ESA Special Publication, 461, ISBN 92-9092-685-6, ESA Publications Division, Noordwijk, Holland.

Richter, A., Burrows, J.P., 2002. Retrieval of tropospheric NO_2 from GOME measurements. Advances in Space Research 29 (11), 1673–1683.

Rozanov, V., Diebel, D., Spurr, R.J.D., Burrows, J.P., 1997. GOMETRAN: a radiative transfer model for the satellite project GOME—the plane parallel version. Journal of Geophysical Research 102, 16683–16696.

Stohl, A., 2001. A 1-year Lagrangian "climatology" of air streams in the Northern Hemisphere troposphere and lowermost stratosphere. Journal of Geophysical Research 106, 7263–7279.

Streets, D.G., Waldhoff, S.T., 2000. Present and future emissions of air pollutants in China: SO_2, NO_x, and CO. Atmospheric Environment 34 (3), 363–374.

Thompson, A.M., Witte, J.C., Hudson, R.D., Guo, H., Herman, J.R., Fujiwara, M., 2001. Tropical tropospheric ozone and biomass burning. Science 291, 2128–2132.

van Aardenne, J.A., Carmichael, G.R., Levy II, H., Streets, D., Hordijk, L., 1999. Anthropogenic NO_x emission in Asia in the period 1990–2020. Atmospheric Environment 33, 633–646.

von Kuhlmann, R., Lawrence, M.G., Crutzen, P.J., Rasch, P.J., 2003a. A model for studies of tropospheric ozone and nonmethane hydrocarbons: model description and ozone results. Journal of Geophysical Research, 108 (D9), 4294 (doi:10.1029/2002JD002893).

von Kuhlmann, R., Lawrence, M.G., Crutzen, P.J., Rasch, P.J., 2003b. A model for studies of tropospheric ozone and nonmethane hydrocarbons: model evaluation of ozone related species. Journal of Geophysical Research, in press (doi:10.1029/2002JD003348).

Wenig, M., 2001. Satellite measurments of long-term global tropospheric trace gas distributions and source strengths—algorithm development and data analysis. Ph.D. Thesis, Rupertus Carola University of Heidelberg.

Yienger, J.J., Levy, H., 1995. Empirical model of global soil-biogenic NO_x emissions. Journal of Geophysical Research 100, 11447–11464.